Harmonic Interaction Analysis in a Grid-Connected Converter Using Harmonic State-Space (HSS) Modeling

JunBum Kwon, *Student Member, IEEE*, Xiongfei Wang, *Member, IEEE*, Frede Blaabjerg, *Fellow, IEEE*, Claus Leth Bak, *Senior Member, IEEE*, Vasile-Simion Sularea, and Cristian Busca, *Member, IEEE*

***Abstract*—An increasing number of power-electronic-based distributed generation systems and loads generate not only characteristic harmonics but also unexpected harmonics. Several methods, such as impedance-based analysis, which are derived from the conventional average model, are introduced to perform research about the harmonic interaction. However, it is found that the linear-time-invariant-based model analysis makes it difficult to analyze these phenomena because of the time-varying properties of the power-electronic-based systems. This paper investigates a grid-connected converter by using the harmonic state-space (HSS) small-signal model, which is based on a linear time-varying periodically theory. The proposed model can include the switching behavior of the model, where it makes the model possible to analyze how harmonics are transferred into both the ac-side and dc-side circuits. Furthermore, a harmonic matrix of the grid-connected converter is developed to analyze the harmonic interaction at the steady-state behavior. Besides, the frequency-domain results are compared with time-domain simulation results by using the HSS modeling to verify the theoretical analysis. Experimental results are finally discussed to verify the proposed model and study.**

***Index Terms*—Harmonic coupling analysis, harmonic state-space (HSS) modeling, three-phase grid-connected converter.**

I. Introduction

With the increased use of power-electronic-based distributed generation (DG) Systems, the stability and the dynamic performance of the system are important issues today [2]–[6]. Particularly, various DG systems are gathered into the same grid network, where complex connections, active control, and bidirectional current flow can make it difficult to analyze the dynamics and interaction of the power-electronic-based systems [3], [7]–[11]. Besides that, even if "*N*" identical power converters, which operate simultaneously or independently, are connected to the same bus, the cancellation, generation, attenuation, and magnification of harmonics are available depending on the randomness [12].

The introduced harmonic interactions mainly occur in power converters, because the ac-side impedance is coupled with the dc-side impedance through the frequency coupling (FC), which is generated by the switching modulation. The variation of harmonics with their negative impact on distribution losses and the possibility of interruption to other customers are main concerns of the network operator [13]. Furthermore, these coupled operations of the system may invoke instability problems in the power-electronic-based systems [5], [14]. Hence, an accurate harmonic analysis of steady-state and dynamic behaviors is important in order to obtain a stable operation of the power systems.

"*Switching method and modulation*" of the power converter, which is the time-varying component in the power converter, should be considered to get the accurate frequency response. However, it is typically neglected or simplified as an averaged duty value in the linear time-invariant (LTI) model with the assumptions where the switching may not affect the behavior of the controller due to the high switching frequency. However, it has been shown in generalized averaging (GAV) and other advanced averaging methods [15]–[17] that the modulation should be taken into account with its phasor in order to achieve an accurate modeling. Additionally, the phasor information of switching and its sideband frequency should also be considered in both low switching frequency (< 2 kHz) and grid-dependent switching application (e.g., diode and thyristor application) in order to investigate their effect on the controller or the interaction with other elements [18], [19]. Hence, the switching components and modulation should be modeled together with other components.

Several methods, which are derived from average-based models, are introduced in [5] and [20]–[22] to investigate these problems, i.e., state-space averaging (SSAV), DQ domain (DQ), and GAV. However, these LTI-based models are not enough to analyze these complex and bidirectional phenomena, because of the time-varying properties of power converter operation and the typically neglected switching modulation during the modeling procedure. For instance, the breaking and normal operation of the converter in railway applications, the discharging and charging of the batteries in energy storage systems, and the different operating point of the converter in renewable energy applications can be the challenges in the analysis of the system using

Manuscript received July 14, 2016; revised October 18, 2016; accepted October 21, 2016. Date of publication December 16, 2016; date of current version April 24, 2017. This work was supported by the European Research Council under the European Union's Seventh Framework Program (FP/2007-2013)/ERC Grant Agreement (321149-Harmony). Recommended for publication by Associate Editor J. H. R. Enslin.

The authors are with the Department of Energy Technology, Aalborg University, Aalborg 9220, Denmark (e-mail: jbk@et.aau.dk; xwa@et.aau.dk; fbl@et.aau.dk; Clb@et.aau.dk: vss@et.aau.dk; cbu@et.aau.dk).

Color versions of one or more of the figures in this paper are available online at http://ieeexplore.ieee.org.

Digital Object Identifier 10.1109/TPEL.2016.2625802

the conventional modeling approaches. As a result, it is found that the FCs, which are driven by the switching modulation, harmonics, and time-varying properties of signals, are the main reasons for the difficulties to analyze the bidirectional systems correctly. Hence, the developments of an accurate model including time-varying signals are important in order to understand the harmonic interaction and the FC of converters [5], [6], [14].

To solve the problems, new modeling approaches considering the periodic signals have been proposed. A harmonic linearization method is introduced in [23] and [24] to calculate the input–output impedance of three-phase systems according to linearized sequence components. Besides, a steady-state analysis of a modular multilevel converter is performed to analyze the circulating current by using Fourier series expansion and small-signal modeling [25], [26]. However, the harmonic interaction in the system with an overall picture of the other components has not been studied. Furthermore, the harmonic interaction problem inside the voltage source converter is also typically overlooked due to a simplified modeling approach [27].

As an alternative to analyze the harmonic couplings at the transmission level, harmonic domain (HD) [28]–[31], extended harmonic domain (EHD) [32]–[38], and harmonic state-space (HSS) [18], [19], [39], [40] modeling methods were introduced in the analysis of the power system. For the steady-state harmonic coupling investigations in symmetrical and unsymmetrical grid conditions, the HD method has been developed [30]. However, this approach was not enough to derive the dynamic behavior of the time domain. Hence, the EHD modeling is introduced to explore the dynamic performance of the HD, where precalculated HD values are used as initial values. Flexible ac transmission system devices [33] as well as wind turbine generators [36] have also been modeled by using the EHD method in order to analyze the transient behaviors of harmonics when the parameters are varied in the simulation. Similarly, the dynamic harmonic domain (DHD) [41]–[43] is also proposed in order to consider a nonlinear characteristic of an inductor and a transformer in the dynamic model of synchronous machines and transmission line [43]. However, both EHD and DHD have mainly discussed the open-loop circuit (fixed switching instant), or the control behavior was numerically taken into account through the numerical methods, i.e., Newton–Raphson's method, by iterating the model until the model reaches to the defined error [18], [44]. Furthermore, they could not include the behavior of switching instant variation (SIV), which propagate the behavior of harmonics from the controller to the topology. On the contrary to them, the HSS modeling and the harmonic transfer function (HTF) method are proposed to analyze the bidirectional harmonic coupling of the Swiss railway system [45] and to meet the overall requirement including harmonic interaction and interharmonic analysis [18], [39], [44], [46].

This paper develops an accurate model of the grid-connected converter by using the HSS modeling method. First, the model differences between LTI and linear time-varying periodically (LTP) are reviewed by comparing the structure and their principles. Second, a detailed procedure of the modeling is described by including how the switching component and harmonics can be involved in the modeling procedure through the HSS modeling. Third, the FC of the converter inside is analyzed by using the developed model. Both dynamic and steady-state harmonic interactions are then analyzed from the grid and load disturbance by using the achieved model. Finally, both simulation and experimental results are included in order to validate the proposed method.

II. Review and Principle of the HSS Modeling

In order to include the previously discussed time-varying phenomena, the HSS modeling based on the HD method is proposed in [30] and [39]. In this section, the general modeling principle of the HSS method is reviewed to adapt the method to the grid-connected converter applications.

A. Basic Modeling Principles

Before discussing the detailed modeling procedure, the difference in the structure between LTI and LTP models is briefly explained in this section [47]–[50]. The terminology used is to describe the various state-space equations based on (1)

$$\dot{x} = Ax + Bu \tag{1}$$

$$\dot{x}\ (t) = \ Ax\,(t) + Bu\,(t) \tag{2}$$

$$\dot{x}\,(t) = A\,(t)\,x\,(t) + B\,(t)\,u\,(t) \tag{3}$$

$$\dot{X}\,(\omega, t) = A\,(\omega) \otimes X\,(\omega, t) + B\,(\omega) \otimes U\,(\omega, t) \tag{4}$$

$$(s + jm\omega_0)\,X_n = \sum_{-\infty}^{\infty} A_{n-m} X_m + \sum_{-\infty}^{\infty} B_{n-m} U_m\,. \tag{5}$$

Practically, all circuits in power-electronic-based systems are nonlinear time-varying systems. However, the system can be represented by the LTI model (2), if the system is linearized at an equilibrium point, where the system parameters (*A* and *B*) are time invariant, but the signals (x and u) are still varying to represent the transient status. On the contrary to (2), nonlinear systems can be represented into (3) if the system is linear time-varying (LTV), where the system parameters (*A* and *B*) are time varying with signals (*x* and *u*). To solve the LTV formulation in the power system, (3) can be transformed into (4) based on the assumption that all circuits are time varying periodically related, by using the linearization procedure according to the periodic trajectory. It is worth to note that the system parameters (*A* and *B*) in (4) are time invariant and the signals (*X* and *U*) have time-varying characteristic dependent on the periodic frequency (ω). Additionally, the parameters and signals are composed of frequency information (Fourier coefficient) and use a convolution method to replace a multiplication in the time domain (3). As an alternative, (4) can be represented into (5) to make the convolution easier, where the convolution in the frequency domain can be obtained by a frequency matrix as the Toeplitz matrix, etc. Finally, the general equation of the HSS model in the frequency domain can be obtained as given in (5). All the used equations in this paper use (5) as a formulation.

The HSS modeling is based on the assumption that all circuit relationships vary periodically in time. If the state transition matrix, input signals, and output signals vary, they cannot be solved by the general state-space equation. Hence, it needs to be linearized, where the model is linearized according to the time-varying trajectories. Based on this theory, all the time-domain signals ($x(t)$) can be represented into (6) in the interval $[t_0, t_0 + T]$, where T is the period of the signal, X_k is the Fourier coefficient, ω_0 is the angular frequency, and k is the harmonic order

$$x(t) = \sum_{k\in\mathbb{Z}} X_k e^{jk\omega_0 t}. \tag{6}$$

Additionally, in order to include the dynamic performance in the time and frequency domains, it is required to use the exponentially modulated periodic (EMP) function as the kernel function (e^{-st}) as shown in the following equation:

$$x(t) = e^{st} \sum_{k\in Z} X_k e^{jk\omega_0 t}. \tag{7}$$

Based on the basic representation of the EMP signal characteristics, it is also possible to derive various mathematical expressions, such as the derivative, integral, and the product of two signals, by a time-varying differential equation of the power converter [19]. Finally, the HSS equation is shown in (8), like in (5), which has a time-invariant state transition matrix ($A - N$) and a time-varying state variable matrix (X), which can be represented by the multiplication of the matrix

$$\begin{aligned}(s + jm\omega_0) X_n &= \sum_{-\infty}^{\infty} A_{n-m} X_m + \sum_{-\infty}^{\infty} B_{n-m} U_m \\ Y_n &= \sum_{-\infty}^{\infty} C_{n-m} X_m + \sum_{-\infty}^{\infty} D_{n-m} U_m.\end{aligned} \tag{8}$$

The important issue is that all matrix rows and columns have the frequency information, and the direct result from the HSS model can be converted into the time-domain by using

$$x(t) = P(t) X \tag{9}$$

where

$$P(t) = \left[e^{-jh\omega_0 t} \cdots e^{-j2\omega_0 t}, e^{-j\omega_0 t}, 1, e^{j\omega_0 t}, e^{j2\omega_0 t} \cdots e^{jh\omega_0 t}\right]$$

$$X = \left[X_{-h}(t) \cdots X_{-1}(t) X_0(t) X_1(t) \cdots X_h(t)\right]^{\mathrm{T}}.$$

Each time-varying Fourier coefficient (X_k) can be rotated at a specific frequency ($e^{-jk\omega_0 t}$), and the summation of all results ($\sum X_k(t) e^{-jk\omega_0 t}$) is the same as the time-domain signal ($x(t)$).

III. HSS Modeling of a Grid-Connected Converter

The block diagram of a three-phase grid-connected converter is shown in Fig. 1. The HSS modeling is performed in two separate parts. First, the topology part as shown in Fig. 1(a) is considered, where a grid-side inductor ($L_g + R_g$), an inverter-side inductor ($L_f + R_f$), and an ac filter capacitor ($C_f + R_{cf}$) are connected to the ac side, and the dc-link capacitor ($C_{\mathrm{dc}} + R_{\mathrm{dc}}$) is connected to the dc-side circuit through a switch network.

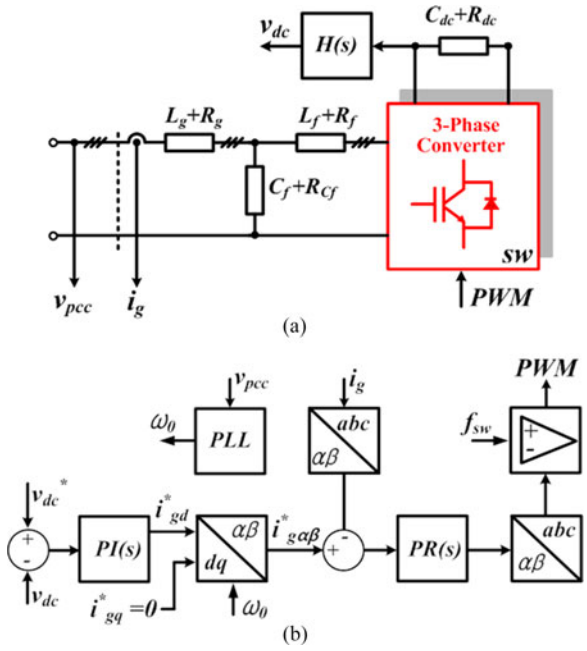

Fig. 1. Block diagram of a three-phase grid-connected converter. (a) Topology. (b) Controller.

Second, the controller part in Fig. 1(b) is modeled by means of the LTP theory. The dc voltage reference (v^*_{dc}) is compared with a sensed dc voltage (v_{dc}) through a low-pass filter (*H(s)*) and the error is controlled by a PI controller (PI*(s)*). The derived *d*-axis current reference (i^*_{gd}) is transformed into alpha–beta coordinates ($i^*_{g\alpha\beta}$) and the references are compared with the transformed sensing current ($i_{g\alpha\beta}$). The errors are compensated by means of a PR controller (PR*(s)*). Finally, the achieved reference frame is retransformed into *abc* coordinates to be compared with a triangle waveform, and the results [pulse width modulation (PWM)] are used to operate switches. The modeling procedure is explained by two parts in the topology and the controller.

A. Topology Modeling

The simple block diagrams in Fig. 1(a) can be decomposed, as shown in Fig. 2, where all acronyms in Fig. 1 have the same meaning, as given in Fig. 1(a). The small-signal representation (Δ) is used in the differential equation to achieve a small-signal-based HSS model. According to the circuit relation described in Fig. 2(a), the ac-side circuit and dc-side circuit can be represented as given in (10)–(14), where v_{capABC} is the ac filter capacitor voltage and other acronyms are used from Figs. 1 and 2

$$\begin{aligned}\frac{d}{dt}\Delta i_{gA} &= \frac{\Delta v_{pccA} - \Delta v_{cfA}}{L_{gA}} - \frac{R_{gA}}{L_{gA}}\Delta i_{gA} \\ \frac{d}{dt}\Delta i_{gB} &= \frac{\Delta v_{pccB} - \Delta v_{cfB}}{L_{gB}} - \frac{R_{gB}}{L_{gB}}\Delta i_{gB} \\ \frac{d}{dt}\Delta i_{gC} &= \frac{\Delta v_{pccC} - \Delta v_{cfC}}{L_{gC}} - \frac{R_{gC}}{L_{gC}}\Delta i_{gC}\end{aligned} \tag{10}$$

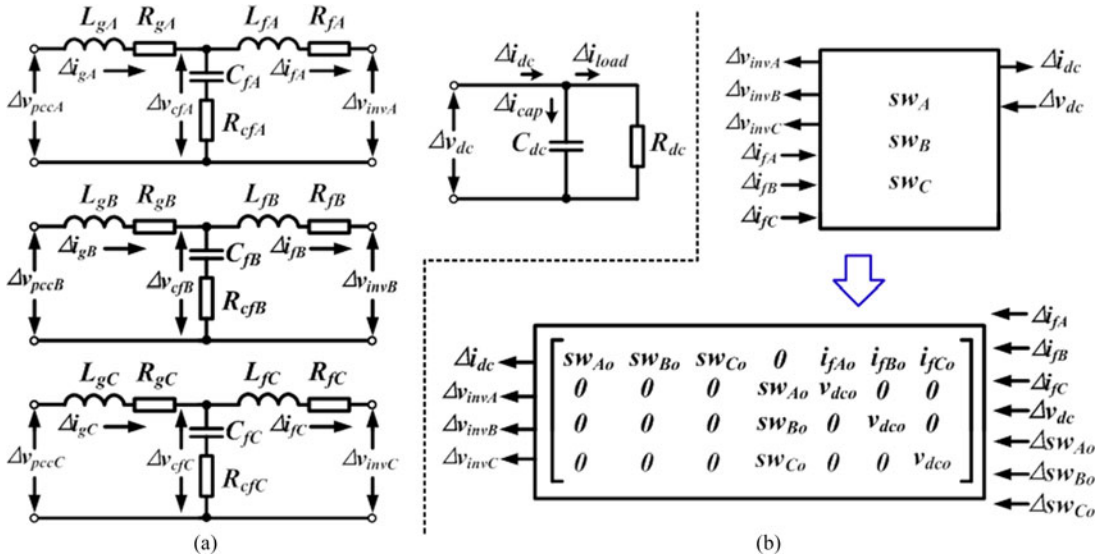

Fig. 2. Linearization of a three-phase grid-connected converter. (a) AC/DC filter. (b) Switching network.

$$\frac{d}{dt}\Delta i_{fA} = \frac{\Delta v_{cfA} - \Delta v_{invA}}{L_{fA}} - \frac{R_{fA}}{L_{fA}}\Delta i_{fA}$$
$$\frac{d}{dt}\Delta i_{fB} = \frac{\Delta v_{cfB} - \Delta v_{invB}}{L_{fB}} - \frac{R_{fB}}{L_{fB}}\Delta i_{fB}$$
$$\frac{d}{dt}\Delta i_{fC} = \frac{\Delta v_{cfC} - \Delta v_{invC}}{L_{fC}} - \frac{R_{fC}}{L_{fC}}\Delta i_{fC} \tag{11}$$

$$\Delta i_{\rm dc} = \frac{\Delta v_{\rm dc}}{R_{\rm dc}} + C_{\rm dc}\frac{d}{dt}\Delta v_{\rm dc} \tag{12}$$

$$\Delta v_{cfA} = \Delta v_{capA} + (\Delta i_{gA} - \Delta i_{fA})\, R_{cfA}$$
$$\Delta v_{cfB} = \Delta v_{capB} + (\Delta i_{gB} - \Delta i_{fB})\, R_{cfB}$$
$$\Delta v_{cfC} = \Delta v_{capC} + (\Delta i_{gC} - \Delta i_{fC})\, R_{cfC} \tag{13}$$

$$\frac{d}{dt}\Delta v_{capA} = \frac{\Delta i_{gA} - \Delta i_{fA}}{C_{fA}}$$
$$\frac{d}{dt}\Delta v_{capB} = \frac{\Delta i_{gB} - \Delta i_{fB}}{C_{fB}}$$
$$\frac{d}{dt}\Delta v_{capC} = \frac{\Delta i_{gC} - \Delta i_{fC}}{C_{fC}}. \tag{14}$$

The switching (sw) generated by PWM and their relationship with the ac- and dc-side circuit can be represented as given in (15), (16) and Fig. 2(b), where the converter-side filter currents (i_{fABC}) are multiplied with the switching (sw) to generate the dc current ($i_{\rm dc}$). The generated dc voltage ($v_{\rm dc}$) is repetitively multiplied with the switching (sw) to supply the converter output voltage (v_{invABC}). Even though the switching (sw) in (15) should be $\mathrm{sw}_{A,B,C} - (\mathrm{sw}_A + \mathrm{sw}_B + \mathrm{sw}_C)/3$, "$(\mathrm{sw}_A + \mathrm{sw}_B + \mathrm{sw}_C)/3$" is neglected, since the summation of three-phase switching is zero when the grid-connected converter is operating under balanced conditions. Furthermore, even though the switching does not have state variable information, it is mainly required to linearize the switching property at a specific operation point to include an SIV driven by the controller behavior. The linearized results are given in (17) and (18) assuming that the switching instant from the controller behavior is very small. The subscript "o" in (17) $\sim$ (18) means a previous state value that can be obtained from nominal value or simulation results. The acronym "Δ" means small variations of signals, which are generated from dynamic controller behavior

$$v_{invA}(t) = v_{\rm dc}(t) sw_A(t)$$
$$v_{invB}(t) = v_{\rm dc}(t) sw_B(t)$$
$$v_{invC}(t) = v_{\rm dc}(t) sw_C(t) \tag{15}$$
$$i_{\rm dc}(t) = i_{fA}(t) sw_A(t) + i_{fB}(t) sw_B(t) + i_{fC}(t) sw_C(t) \tag{16}$$

$$\Delta v_{invA}(t) = \mathrm{sw}_{Ao}\Delta v_{\rm dc} + v_{dco}\Delta \mathrm{sw}_A$$
$$\Delta v_{invB}(t) = \mathrm{sw}_{Bo}\Delta v_{\rm dc} + v_{dco}\Delta \mathrm{sw}_B$$
$$\Delta v_{invC}(t) = \mathrm{sw}_{Co}\Delta v_{\rm dc} + v_{dco}\Delta \mathrm{sw}_C \tag{17}$$
$$\Delta i_{\rm dc} = \mathrm{sw}_{Ao}\Delta i_{fA} + i_{fAo}\Delta \mathrm{sw}_A + \mathrm{sw}_{Bo}\Delta i_{fB} + i_{fBo}\Delta \mathrm{sw}_B + \mathrm{sw}_{Co}\Delta i_{fC} + i_{fCo}\Delta \mathrm{sw}_C. \tag{18}$$

The small-signal and the differential equations (10)–(14) can be transformed into the state-space equation as given by (19) by substituting (17) and (18) into (11) and (12)

$$\dot{x}_t = A_t\, x_t + B_t u_t \tag{19}$$

where $x_t = [\Delta i_{gA}\Delta i_{gB}\ \Delta i_{gC}\ \Delta v_{capA}\ \Delta v_{capB}\ \Delta v_{capC}\ \Delta i_{fA}\ \Delta i_{fB}\ \Delta i_{fC}\ \Delta v_{\rm dc}]^T$, $u_t = [\Delta v_{pccA}\ \Delta v_{pccB}\ \Delta v_{pccC}\ \ \Delta \mathrm{sw}_A\ \Delta \mathrm{sw}_B\ \Delta \mathrm{sw}_C]^T$, and A_t and B_t are given in (20) and (21),

$$A_t = \begin{bmatrix} \frac{-R_{gA}-R_{cfA}}{L_{gA}} & 0 & 0 & \frac{-1}{L_{gA}} & 0 & 0 & \frac{R_{cfA}}{L_{gA}} & 0 & 0 & 0 \\ 0 & \frac{-R_{gB}-R_{cfB}}{L_{gB}} & 0 & 0 & \frac{-1}{L_{gB}} & 0 & 0 & \frac{R_{cfB}}{L_{gB}} & 0 & 0 \\ 0 & 0 & \frac{-R_{gC}-R_{cfC}}{L_{gC}} & 0 & 0 & \frac{-1}{L_{gC}} & 0 & 0 & \frac{R_{cfC}}{L_{gC}} & 0 \\ \frac{1}{C_{fA}} & 0 & 0 & 0 & 0 & 0 & \frac{-1}{C_{fA}} & 0 & 0 & 0 \\ 0 & \frac{1}{C_{fB}} & 0 & 0 & 0 & 0 & 0 & \frac{-1}{C_{fB}} & 0 & 0 \\ 0 & 0 & \frac{1}{C_{fC}} & 0 & 0 & 0 & 0 & 0 & \frac{-1}{C_{fC}} & 0 \\ \frac{R_{cfA}}{L_{fA}} & 0 & 0 & \frac{1}{L_{fA}} & 0 & 0 & \frac{-R_{fA}-R_{cfA}}{L_{fA}} & 0 & 0 & \frac{-\mathrm{sw}_{Ao}}{L_{fA}} \\ 0 & \frac{R_{cfB}}{L_{fB}} & 0 & 0 & \frac{1}{L_{fB}} & 0 & 0 & \frac{-R_{fB}-R_{cfB}}{L_{fB}} & 0 & \frac{-\mathrm{sw}_{Bo}}{L_{fB}} \\ 0 & 0 & \frac{R_{cfC}}{L_{fC}} & 0 & 0 & \frac{1}{L_{fC}} & 0 & 0 & \frac{-R_{fC}-R_{cfC}}{L_{fC}} & \frac{-\mathrm{sw}_{Co}}{L_{fC}} \\ 0 & 0 & 0 & \frac{\mathrm{sw}_{Ao}}{C_{\mathrm{dc}}} & \frac{\mathrm{sw}_{Bo}}{C_{\mathrm{dc}}} & \frac{\mathrm{sw}_{Co}}{C_{\mathrm{dc}}} & 0 & 0 & 0 & \frac{-1}{R_{\mathrm{dc}}C_{\mathrm{dc}}} \end{bmatrix} \tag{20}$$

respectively: (20) as shown at the top of the page

$$B_t = \begin{bmatrix} \frac{1}{L_{gA}} & 0 & 0 & 0 & 0 & 0 \\ 0 & \frac{1}{L_{gB}} & 0 & 0 & 0 & 0 \\ 0 & 0 & \frac{1}{L_{gC}} & 0 & 0 & 0 \\ 0 & 0 & 0 & 0 & 0 & 0 \\ 0 & 0 & 0 & 0 & 0 & 0 \\ 0 & 0 & 0 & 0 & 0 & 0 \\ 0 & 0 & 0 & \frac{-v_{dco}}{L_{fA}} & 0 & 0 \\ 0 & 0 & 0 & 0 & \frac{-v_{dco}}{L_{fA}} & 0 \\ 0 & 0 & 0 & 0 & 0 & \frac{-v_{dco}}{L_{fA}} \\ 0 & 0 & 0 & \frac{i_{fAo}}{C_{\mathrm{dc}}} & \frac{i_{fBo}}{C_{\mathrm{dc}}} & \frac{i_{fCo}}{C_{\mathrm{dc}}} \end{bmatrix}. \tag{21}$$

As a result, (19)–(21) should be converted into the LTP formulation according to the assumption that all signals are varying periodically and they can be linearized in periodic trajectories. Hence, (22)–(24) can be obtained by using the HSS modeling procedure that is introduced in (6)–(9)

$$\dot{X}_f = A_f X_f + B_f U_f \tag{22}$$

where $X_f = [\Delta I_{gA}\Delta I_{gB}\Delta I_{gC}\Delta V_{capA}\Delta V_{capB}\Delta V_{capC}\Delta I_{fA}\ \Delta I_{fB}\ \Delta I_{fC}\ \Delta V_{\mathrm{dc}}]^T$, $U_f = [\Delta V_{pccA}\ \Delta V_{pccB}\ \Delta V_{pccC}\ \Delta \mathrm{SW}_A \Delta \mathrm{SW}_B\ \Delta \mathrm{SW}_C{}^T$, and A_f and B_f are given in (23) and (24), respectively. The small letter in (19)–(21) means the time-domain signal. The capital letters in (22)–(24) are the harmonic coefficient component from $[\ldots -h \ldots -1, 0, 1 \ldots h \ldots]$, which is derived from the Fourier series. In this paper, -20th–20th harmonics orders are considered to analyze the harmonic interaction by the 20th harmonics (23) as shown at the top of the next page

$$B_f = \begin{bmatrix} \frac{1}{L_{gA}}I & Z_M & Z_M & Z_M & Z_M & Z_M \\ Z_M & \frac{1}{L_{gB}}I & Z_M & Z_M & Z_M & Z_M \\ Z_M & Z_M & \frac{1}{L_{gC}}I & Z_M & Z_M & Z_M \\ Z_M & Z_M & Z_M & Z_M & Z_M & Z_M \\ Z_M & Z_M & Z_M & Z_M & Z_M & Z_M \\ Z_M & Z_M & Z_M & Z_M & Z_M & Z_M \\ Z_M & Z_M & Z_M & \frac{-\Gamma[V_{\mathrm{dc0}}]}{L_{fA}} & Z_M & Z_M \\ Z_M & Z_M & Z_M & Z_M & \frac{-\Gamma[V_{\mathrm{dc0}}]}{L_{fB}} & Z_M \\ Z_M & Z_M & Z_M & Z_M & Z_M & \frac{-\Gamma[V_{\mathrm{dc0}}]}{L_{fC}} \\ Z_M & Z_M & Z_M & \frac{\Gamma[I_{fAo}]}{C_{\mathrm{dc}}} & \frac{\Gamma[I_{fBo}]}{C_{\mathrm{dc}}} & \frac{\Gamma[I_{fCo}]}{C_{\mathrm{dc}}} \end{bmatrix}. \tag{24}$$

The direct results from (22) can be retransformed into the time-domain signal by using (9) according to the principle of LTP. Additionally, "I" denotes the identity matrix, "Z_M" is zero matrix having the same matrix size with the considered number of harmonics, and "$N = \mathrm{diag}[-jh\omega_0 \ldots -j\omega_0, 0, j\omega_0 \ldots jh\omega_0]$" is derived from the derivative procedure of (8). The previous values of the time-domain switching functions (sw_{ABCo}), ac filter current (i_{fABCo}), and dc voltage (v_{dco}) are reorganized into a Toeplitz (Γ)matrix [18] in order to perform a convolution. The multiplication of two time-domain signals can be implemented into the frequency domain by means of a convolution, where this can be obtained by using the Toeplitz matrix and the harmonic vectors. The derived output harmonic vector from the Toeplitz matrix can be converted into time-domain signals by using (9).

Conclusively, the topology in Fig. 1(a) is modeled as (22) by using the HSS modeling method. The derived result can show how a small variation of the input harmonics

$$\mathrm{A_f}=\begin{bmatrix}
\frac{-R_{gA}-R_{cfA}}{L_{gA}}I-N & Z_M & Z_M & \frac{-1}{L_{gA}}I & Z_M & Z_M & \frac{R_{cfA}}{L_{gA}}I & Z_M & Z_M & Z_M\\
Z_M & \frac{-R_{gB}-R_{cfB}}{L_{gB}}I-N & Z_M & Z_M & \frac{-1}{L_{gB}}I & Z_M & Z_M & \frac{R_{cfB}}{L_{gB}}I & Z_M & Z_M\\
Z_M & Z_M & \frac{-R_{gC}-R_{cfC}}{L_{gC}}I-N & Z_M & Z_M & \frac{-1}{L_{gC}}I & Z_M & Z_M & \frac{R_{cfC}}{L_{gC}}I & Z_M\\
\frac{1}{C_{fA}}I & Z_M & Z_M & -N & Z_M & Z_M & \frac{-1}{C_{fA}}I & Z_M & Z_M & Z_M\\
Z_M & \frac{1}{C_{fB}}I & Z_M & Z_M & -N & Z_M & Z_M & \frac{-1}{C_{fB}}I & Z_M & Z_M\\
Z_M & Z_M & \frac{1}{C_{fC}}I & Z_M & Z_M & -N & Z_M & Z_M & \frac{-1}{C_{fC}}I & Z_M\\
\frac{R_{cfA}}{L_{fA}}I & Z_M & Z_M & \frac{1}{L_{fA}}I & Z_M & Z_M & \frac{-R_{fA}-R_{cfA}}{L_{fA}}I-N & Z_M & Z_M & \frac{-\Gamma[SW_{Ao}]}{L_{fA}}\\
Z_M & \frac{R_{cfB}}{L_{fB}}I & Z_M & Z_M & \frac{1}{L_{fB}}I & Z_M & Z_M & \frac{-R_{fB}-R_{cfB}}{L_{fB}}I-N & Z_M & \frac{-\Gamma[SW_{Bo}]}{L_{fB}}\\
Z_M & Z_M & \frac{R_{cfC}}{L_{fC}}I & Z_M & Z_M & \frac{1}{L_{fC}}I & Z_M & Z_M & \frac{-R_{fC}-R_{cfC}}{L_{fC}}I-N & \frac{-\Gamma[SW_{Co}]}{L_{fC}}\\
Z_M & Z_M & Z_M & \frac{\Gamma[SW_{Ao}]}{C_{dc}} & \frac{\Gamma[SW_{Bo}]}{C_{dc}} & \frac{\Gamma[SW_{Co}]}{C_{dc}} & Z_M & Z_M & Z_M & \frac{-1}{R_{dc}C_{dc}}I-N
\end{bmatrix} \tag{23}$$

$(\Delta V_{pccABC},\ \Delta \mathrm{SW}_{ABC})$ can be transferred into output harmonic information $(\Delta I_{gABC},\ \Delta I_{fABC},\ \Delta V_{capABC},\ \Delta V_{\mathrm{dc}})$.

B. Controller Modeling

Based on Fig. 1(b), the controller can also be modeled by using a time-domain differential equation to frequency-domain differential equation transformation. The small-signal representation (Δ) is used to obtain small variations of the switching $(\Delta \mathrm{SW}_{ABC})$ from the controller output. The phase-locked loop is assumed to provide a steady-state angle information (θ_0) to both current controller and park transformation. Additionally, the Clarke's transformation in the time domain can be represented as given in (25) and (26) in the frequency domain as

$$\mathrm{clark}_{abc-\alpha\beta}=\begin{bmatrix}\frac{2}{3} & -\frac{1}{3} & -\frac{1}{3}\\ 0 & \frac{1}{\sqrt{3}} & -\frac{1}{\sqrt{3}}\end{bmatrix} \tag{25}$$

$$\mathrm{CLARK}_{abc-\alpha\beta}=\begin{bmatrix}\frac{2}{3}I & -\frac{1}{3}I & -\frac{1}{3}I\\ Z_M & \frac{1}{\sqrt{3}}I & -\frac{1}{\sqrt{3}}I\end{bmatrix} \tag{26}$$

where (25) is for time-domain transformation and (26) is for transformation into the frequency domain. The inputs of (26) are the Fourier coefficient components derived from sensed signals or from other outputs. In a similar way, Park's transformation in the time and frequency domains can be represented as given in (27) and (28). The different aspect of Clarke's transformation is that Park's transformation is a multiplication of two time-domain signals. Hence, the convolution theory, which is explained in the previous section, is also used in the transformation

$$\mathrm{park}_{\alpha\beta}=\begin{bmatrix}\cos(\theta_0) & \sin(\theta_0)\\ -\sin(\theta_0) & \cos(\theta_0)\end{bmatrix}$$

$$\mathrm{PARK}_{\alpha\beta}=\begin{bmatrix}\Gamma[\cos(\theta_o)] & \Gamma[\sin(\theta_o)]\\ -\Gamma[\sin(\theta_o)] & \Gamma[\cos(\theta_o)]\end{bmatrix} \tag{27}$$

$$=\begin{bmatrix}\Gamma\left[\cdots\frac{1}{2},0,\frac{1}{2},\cdots\right] & \Gamma\left[\cdots-\frac{1}{j2},0,\frac{1}{j2},\cdots\right]\\ -\Gamma\left[\cdots-\frac{1}{j2},0,\frac{1}{j2},\cdots\right] & \Gamma\left[\cdots\frac{1}{2},0,\frac{1}{2},\cdots\right]\end{bmatrix} \tag{28}$$

where "Γ" means a Toeplitz matrix to perform a convolution of two signals, and components in Toeplitz matrix mean the Fourier coefficient components of "$\cos(\theta_0)$" and "$\sin(\theta_0)$"

$$\mathrm{PI}(s)=K_p+\frac{K_i}{s} \tag{29}$$

$$\mathrm{PR}(s)=K_{\mathrm{pPR}}+\frac{sK_{\mathrm{iPR}}}{s^2+\omega_0^2} \tag{30}$$

$$H(s)=\frac{1}{K_{\mathrm{LPF}}s+1} \tag{31}$$

where K_p and K_i are proportional and integral gains used in the PI controller, respectively, K_{pPR} and K_{iPR} are PR controller gains employed in both α- and β-axis, respectively, and K_{LPF} is a low-pass filter gain used for the sensing and filtering of dc voltage (v_{dc}). As a result, the HSS model for the controller part can be derived as given in (32) by using Fig. 1(b), (26), (28), and (29)–(31), where the capital letter means a Fourier coefficient $(+\ldots-)$ and acronyms in (22) have the same meaning with topology modeling in Fig. 2

$$\begin{aligned}\dot{X}_{fc}&=A_{fc}X_{fc}+B_{fc}U_{fc}\\ Y_{fc}&=C_{fc}X_{fc}+D_{fc}U_{fc}\end{aligned} \tag{32}$$

where $X_{fc}=[\Delta X_{\mathrm{LPF}}\ \Delta X_{\mathrm{PI}}\ \Delta X_{\mathrm{PR}\alpha1}\ \Delta X_{\mathrm{PR}\alpha2}\ \Delta X_{\mathrm{PR}\beta1}\ \Delta X_{\mathrm{PR}\beta2}]^T$, $U_{fc}=[\Delta V_{\mathrm{dc}}\ \Delta V_{\mathrm{dc}}^*\ \Delta I_{ga}\ \Delta I_{gb}\ \Delta I_{gc}]^T$, $Y_{fc}=[\Delta \mathrm{SW}_A\ \Delta \mathrm{SW}_B\ \Delta \mathrm{SW}_C]^T$, ΔX_{LPF} is the harmonic state variable of a low-pass filter [$H(s)$] shown in Fig. 1(a), ΔX_{PI} is the state variable of the PI controller [PI(s)], and $\Delta X_{\mathrm{PR}\alpha1},\ \Delta X_{\mathrm{PR}\alpha2},\ \Delta X_{\mathrm{PR}\beta1}$, and $\Delta X_{\mathrm{PR}\beta2}$ are state variables used in the PR controller [PR(s)] at α- and β-axes, and

A_{fc}, B_{fc}, C_{fc}, and D_{fc} are given in (33)–(36), respectively

$$A_{fc}=\begin{bmatrix} -\dfrac{1}{K_{\mathrm{LPF}}}I-N & Z_M & Z_M & Z_M & Z_M & Z_M \\ -I & -N & Z_M & Z_M & Z_M & Z_M \\ -K_p\Gamma\left[\cos\left(\theta_o\right)\right] & K_i\Gamma\left[\cos\left(\theta_o\right)\right] & -N & -\omega_0^2 I & Z_M & Z_M \\ Z_M & Z_M & I & -N & Z_M & Z_M \\ -K_p\Gamma\left[\cos\left(\theta_o\right)\right] & K_i\Gamma\left[\sin\left(\theta_o\right)\right] & Z_M & Z_M & -N & -\omega_0^2 I \\ Z_M & Z_M & Z_M & Z_M & I & -N \end{bmatrix} \tag{33}$$

$$B_{fc}=\begin{bmatrix} \dfrac{1}{K_{\mathrm{LPF}}}I & Z_M & Z_M & Z_M & Z_M \\ Z_M & I & Z_M & Z_M & Z_M \\ Z_M & K_p\Gamma\left[\cos\left(\theta_o\right)\right] & -\dfrac{2}{3}I & \dfrac{1}{3}I & \dfrac{1}{3}I \\ Z_M & Z_M & Z_M & Z_M & Z_M \\ Z_M & K_p\Gamma\left[\sin\left(\theta_o\right)\right] & Z_M & -\dfrac{1}{\sqrt{3}}I & \dfrac{1}{\sqrt{3}}I \\ Z_M & Z_M & Z_M & Z_M & Z_M \end{bmatrix} \tag{34}$$

$$C_{fc}=\begin{bmatrix} C_{fc1} & C_{fc2} & K_{\mathrm{iPR}}I & Z_M & Z_M & Z_M \\ C_{fc3} & C_{fc4} & -\dfrac{K_{\mathrm{iPR}}}{2}I & Z_M & \dfrac{\sqrt{3}}{2}K_{\mathrm{iPR}}I & Z_M \\ C_{fc5} & C_{fc6} & -\dfrac{K_{\mathrm{iPR}}}{2}I & Z_M & -\dfrac{\sqrt{3}}{2}K_{\mathrm{iPR}}I & Z_M \end{bmatrix} \tag{35}$$

where

$$C_{fc1}=-K_{\mathrm{pPR}}K_p\Gamma\left[\cos\left(\theta_0\right)\right]$$
$$C_{fc2}=K_{\mathrm{pPR}}K_i\Gamma\left[\cos\left(\theta_0\right)\right]$$
$$C_{fc3}=\frac{1}{2}K_pK_{\mathrm{pPR}}\Gamma\left[\cos\left(\theta_0\right)\right]-\frac{\sqrt{3}}{2}K_pK_{\mathrm{pPR}}\Gamma\left[\sin\left(\theta_0\right)\right]$$
$$C_{fc4}=\frac{\sqrt{3}}{2}K_iK_{\mathrm{pPR}}\Gamma\left[\sin\left(\theta_0\right)\right]-\frac{1}{2}K_iK_{\mathrm{pPR}}\Gamma\left[\cos\left(\theta_0\right)\right]$$
$$C_{fc5}=\frac{1}{2}K_pK_{\mathrm{pPR}}\Gamma\left[\cos\left(\theta_0\right)\right]+\frac{\sqrt{3}}{2}K_pK_{\mathrm{pPR}}\Gamma\left[\sin\left(\theta_0\right)\right]$$
$$C_{fc6}=-\frac{1}{2}K_iK_{\mathrm{pPR}}\Gamma\left[\cos\left(\theta_0\right)\right]-\frac{\sqrt{3}}{2}K_iK_{\mathrm{pPR}}\Gamma\left[\sin\left(\theta_0\right)\right]$$

$$D_{fc}=\begin{bmatrix} Z_M & K_{\mathrm{pPR}}K_p\Gamma\left[\cos\left(\theta_0\right)\right] & -\dfrac{2}{3}K_{\mathrm{pPR}}I & \dfrac{K_{\mathrm{pPR}}}{3}I & \dfrac{K_{\mathrm{pPR}}}{3}I \\ Z_M & D_{fc1} & D_{fc2} & D_{fc3} & D_{fc4} \\ Z_M & D_{fc5} & D_{fc6} & D_{fc7} & D_{fc8} \end{bmatrix} \tag{36}$$

where

$$D_{fc1}=\frac{\sqrt{3}}{2}K_{\mathrm{pPR}}K_p\Gamma\left[\sin\left(\theta_0\right)\right]-\frac{1}{2}K_{\mathrm{pPR}}K_p\Gamma\left[\cos\left(\theta_0\right)\right]$$
$$D_{fc2}=\frac{1}{3}K_{\mathrm{pPR}}I-\frac{1}{\sqrt{3}}K_{\mathrm{pPR}}I$$
$$D_{fc3}=-\frac{1}{6}K_{\mathrm{pPR}}I+\frac{1}{2\sqrt{3}}K_{\mathrm{pPR}}I$$
$$D_{fc44}=-\frac{1}{6}K_{\mathrm{pPR}}I+\frac{1}{2\sqrt{3}}K_{\mathrm{pPR}}I$$
$$D_{fc5}=-\frac{\sqrt{3}}{2}K_{\mathrm{pPR}}K_p\Gamma\left[\sin\left(\theta_0\right)\right]-\frac{1}{2}K_{\mathrm{pPR}}K_p\Gamma\left[\cos\left(\theta_0\right)\right]$$
$$D_{fc6}=\frac{1}{3}K_{\mathrm{pPR}}I+\frac{1}{\sqrt{3}}K_{\mathrm{pPR}}I$$
$$D_{fc7}=-\frac{1}{6}K_{\mathrm{pPR}}I-\frac{1}{2\sqrt{3}}K_{\mathrm{pPR}}I$$
$$D_{fc8}=-\frac{1}{6}K_{\mathrm{pPR}}I-\frac{1}{2\sqrt{3}}K_{\mathrm{pPR}}I.$$

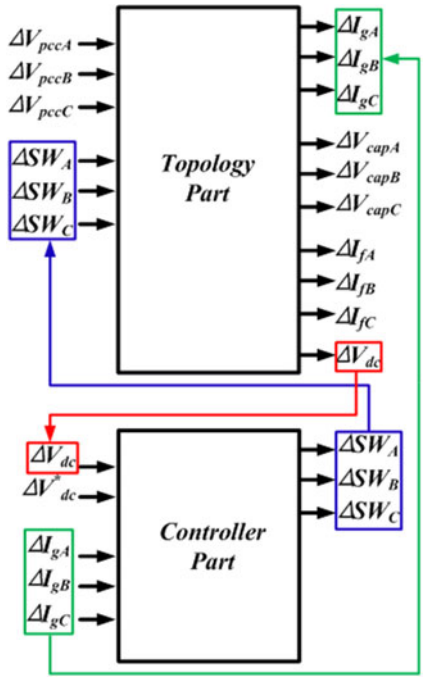

Fig. 3. Connection of two HSS models [Topology part (22) and Controller part (32)].

It is worth to mention that all state variables, inputs, and output are harmonic vectors, and the size of each matrix components is the same as the number of harmonics used in the modeling procedure. Additionally, the switching harmonics and sideband frequency of switching frequency are used to investigate the effect of harmonic interaction driven by them. As a conclusion for the HSS model of the topology (22), where the output vector of (22) can be chosen by the user, and controller HSS model (32) can be connected, as shown in Fig. 3, to transfer harmonic vector each other. The results of the two combined HSS models are all frequency information. However, the frequency outputs can be converted into time-domain results by using (9).

IV. Simulation and Experimental Validation

The full HSS model derived from Section IV is simulated and compared with experimental results. First, steady-state and dynamic simulations of the HSS method are performed by using the harmonic transfer matrix, which is also called the HTF,

and compared with results from the commercial simulation tool (PLECS) in order to validate the accuracy as well as the harmonic transfer procedure of the HSS model. Also, the results are compared with experimental results under the same condition.

A. Simulation and Experimental Conditions

The HSS model is implemented by using an m-file in MATLAB, and laboratory tests are performed in an experimental setup. The control algorithms are implemented in a DS1007 dSPACE system. A three-phase frequency drive is selected as a grid-connected converter at a 3-kW power rating, where the converter-side inductor $L_f = 6.25\,\mathrm{mH}$, the grid-side inductor $L_g = 3.3\,\mathrm{mH}$, the filter capacitance $C_f = 9.4\,\mu\mathrm{F}$, the dc link capacitor $= 450\,\mu\mathrm{F}$, the dc-link voltage $= 750\,\mathrm{V}$, the line–line grid voltage $= 380\,\mathrm{V}$, and the switching frequency $= 2\,\mathrm{kHz}$ are used in both simulations and experiments.

According to the international standard IEC 61000-2-4, which defines the compatibility levels in industrial plants for low-frequency disturbances and applies for low voltage and medium voltage at 50 or 60 Hz, a distorted grid voltage is considered in the simulations as well as in the experiments. In the case of the experiment, a programmable ac source is used to generate a distorted grid voltage condition. The verification of the modeling is also performed under the distorted grid voltage, where case A has third (0.5%), fifth (4.5%), and seventh (0.7%) harmonic distortions and case B has third (0.5%), fifth (2.5%), and seventh (4.5%) harmonic distortions.

The comparison is performed under two specific conditions in order to study the steady state and the dynamics of the harmonics. First, the steady-state behavior of harmonics is investigated. Second, the dynamic behavior of the harmonics is investigated by adjusting the reference at a given instant. It is worth to note that all reproduced signals from the HSS model are using (9). The summation of each sinusoidal signal is, thus, a final time-domain signal, which can be compared with the signals from the time-domain simulation. For instance, the state vectors $X_f = [\Delta I_{gA}\,\Delta I_{gB}\,\Delta I_{gC}\,\Delta V_{capA}\,\Delta V_{capB}\,\Delta V_{capC}\,\Delta I_{fA}\,\Delta I_{fB}\,\Delta I_{fC}\,\Delta V_{\mathrm{dc}}]^T$ of the topology model are composed of the harmonic vector. ΔI_{gA} can be regarded as X in (9), and it can be a single time-domain signal by rotating their components with $P(t)$ in (9). The other harmonic vectors can also be reproduced by using the same manner. Additionally, in order to identify the source of distorted current, the converter is controlled without considering the harmonic compensator in both simulations and experiments.

B. Simulation and Experiment Results

The dynamic behaviors of harmonics from the HSS model are simulated in Fig. 4. The grid-connected converter operates at the condition of "case A" until 0.5 s, and the harmonics in grid voltage are adjusted to "case B" after 0.5 s. The low-order harmonics are mainly depicted in Fig. 4 for the visibility. The grid current is distorted according to the condition of harmonics in the grid voltage. The waveform of the grid current is changed due to the harmonic contents of grid voltage, where fifth and seventh harmonics are adjusted in "case A" and "case B," as shown in Fig. 4(a). Furthermore, the magnitude of harmonics in the dc voltage, as well as in the dc current, is also changed because of the harmonic components in the grid current, where the magnitude of sixth harmonics is mainly changed in the simulations. It is noted that the simulation results in the time domain can also be performed by a commercial simulation tool. However, it is difficult to investigate their coupling by using the conventional tools for modeling. The dynamic couplings are simulated, as shown in Fig. 4(b). The output results of the HSS model at low-order harmonics are mainly drawn for the visibility. The behaviors of the fifth- and seventh-order harmonics are mainly investigated, since the grid voltage is distorted according to "case A" and "case B." The harmonic components in the three-phase grid current are depicted by positive-sequence and negative-sequence harmonics according to the relationship given as

$$\begin{aligned} V_{inv[\mathrm{P}]} &= \mathrm{SW}_{[\mathrm{P}]} * V_{\mathrm{dc}[\mathrm{Z}]} \\ V_{inv[\mathrm{N}]} &= \mathrm{SW}_{[\mathrm{N}]} * V_{\mathrm{dc}[\mathrm{Z}]} \\ I_{dc[\mathrm{Z}]} &= \mathrm{SW}_{[\mathrm{P}]} * I_{g[\mathrm{N}]} + \mathrm{SW}_{[\mathrm{N}]} * I_{g[\mathrm{P}]}. \end{aligned} \tag{37}$$

If it is assumed that there are not zero sequence in the grid side, the procedure of harmonic transfer in the three-phase converter can simply be explained by using (37), where "P" is positive-sequence harmonics [. . . –17, –11, –5, +1, +7, +13 . . .], "N" is negative-sequence harmonics [. . . –13, –7, –1, +5, +11, +17 . . .], "Z" is zero-sequence harmonics [. . . –18, –12, –6, 0, +6, +12, +18 . . .], and "$*$" means the convolution in the frequency domain, and other acronyms are the same as specified in Fig. 3. The convolution between the zero-sequence harmonics in the dc side and positive-sequence harmonics of the switching generates positive-sequence harmonics in the input side of the ac filter, and the negative-sequence harmonics behave similarly. They generate a positive- and negative-sequence harmonics of the grid current through the voltage difference with the positive- and negative-sequence harmonics of the grid voltage. The negative-sequence harmonics of the grid current is convoluted with the positive sequence of the switching component, and the summation of the convolution of the negative-sequence part generates a zero sequence of the dc current. It is used to make the zero sequence of the dc voltage. These procedures happens continuously during the operation.

As a result, the magnitude of the fifth harmonics in positive sequence (–5th) and negative sequence (+5th) decreases as the fifth harmonics of the grid voltage varies. Besides, the magnitude of seventh harmonics at positive sequence (+7th) and negative sequence (–7th) increases as the seventh-order harmonics in the grid voltage increases. It is worth to note that the dc-side harmonics also change simultaneously since the ac side of the converter is coupled with the dc side of the converter through the modulation behavior. The zero-sequence harmonics (+6th/–6th) at the dc side decrease. Additionally, the harmonic vectors in Fig. 4(b) can be converted into Fig. 4(a) by using (9). Each harmonic has their own impedance, and it is coupled with each other, since it has its own transient behavior, as shown in Fig. 4(b). The simulated characteristics mean that the

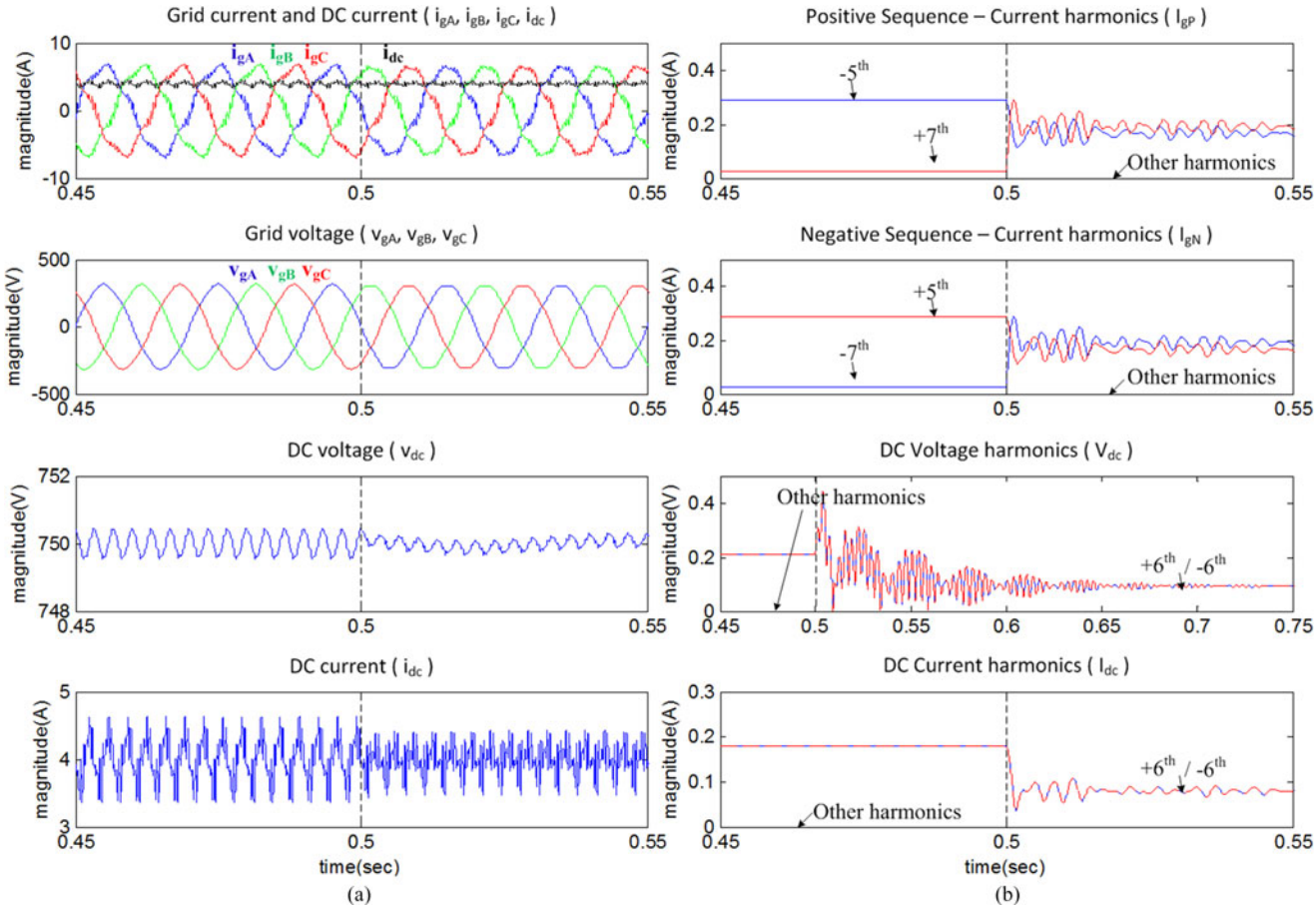

Fig. 4. Simulation result for the verification of harmonic interaction. (a) Time-domain simulation using the HSS method. (b) Dynamic response for harmonic interaction in the time domain.

impedance of harmonics and their transient behaviors are also correlated with the overall behavior of the converter, and the main harmonic impedance should be considered for an accurate analysis.

The harmonics at steady state are compared using the HSS model, PLECS, and experiments. The results of the HSS model are converted to the time domain by using (9), since the output of the HSS model is frequency vectors. The harmonics from –40th to 40th are considered in the HSS model to investigate the low-order harmonics and to show the switching behavior in the time-domain result. Even though five or ten times of the switching frequency may affect the low-order harmonics, the effects of them are very small due to the attenuation by a filter inductor except some special cases [51], [52]. Hence, this paper considered the harmonics up to the switching frequency in order to focus on relatively bigger harmonics. However, more harmonics can be considered in the HSS model if the test object is under the special cases or the user wants to investigate the influence of the switching harmonics. Additionally, the size of the model depends on the harmonics of the modeling procedure. However, it can be reduced according to the requirement. For instance, the positive and negative sequences can only be used for the reduced-order model. As shown in Fig. 5(a) and (b), a comparison between the HSS and PLECS seems to show a good match. It is worth to note that each sequence has a half value of total fast Fourier transform (FFT) values. Hence, the summation of positive sequence and negative sequence in case A [see Fig. 4(b)] shows the same value with Fig. 5(a). The simulation results of case B in Fig. 4(b) can also be compared with Fig. 5(b) through the same manner. The small error can be regarded as a calculation error in the computer simulations or a resolution problem (time step). It is worth to note that the transfer procedure of the harmonics is properly working in the model inside according to the theory of the HSS model. Even though the average model can be used to analyze the harmonic contents of a voltage-source converter, when the switching frequency is very high, it cannot be properly adapted to the harmonic analysis, as the switching frequency is lower ($< 2\,\mathrm{kHz}$). The switching harmonics can be moved to near the low-frequency range and can affect both the dc and ac harmonic transfer procedures through the FC [53]. It means that the impedances of each harmonic are coupled with each other, and it can only be analyzed by the modeling methods, which consider the effect of the time-varying elements. It is worth to note that the HSS model fundamentally adapts the results of rotating frame inside, since the linearized results according to the time-varying trajectory show varying phasors at the end. Hence, the meanings of the Park's and the Clark's transform in the HSS model have a sort of phase shift and

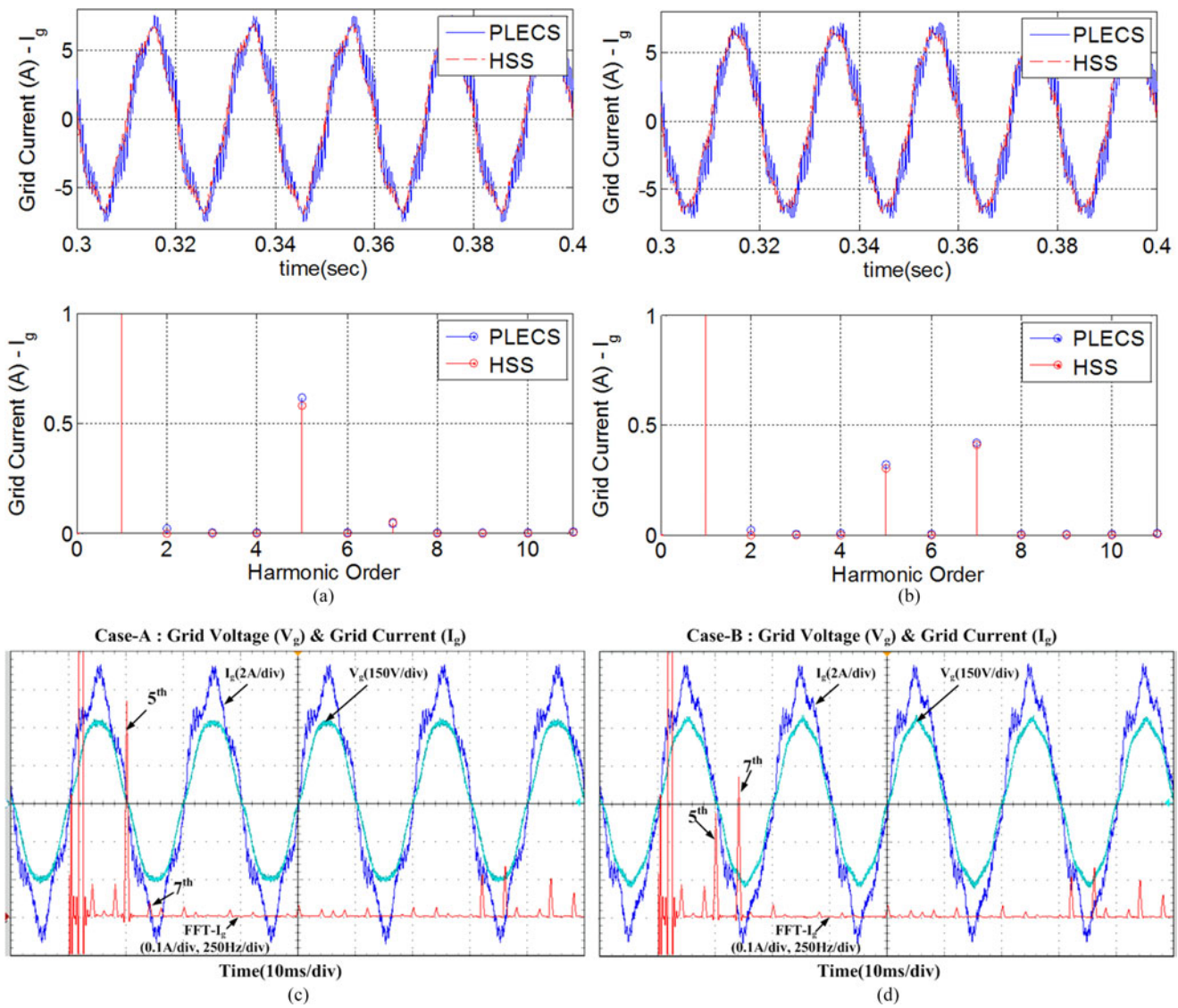

Fig. 5. Simulation (HSS, PLECS) and experimental results. Grid-side inductor current simulation ($\mathrm{harmonic} = -40\mathrm{th} - 40\mathrm{th}$) waveform and FFT from distorted grid voltage: (a) case A and (b) case B (blue = PLECS, red = HSS). Grid-side inductor current experimental waveform and FFT from distorted grid voltage: (c) case A and (d) case B (blue = grid-side current, cyan = grid voltage, red = FFT waveform of grid-side current).

result in the phasor as well. Conclusively, the simulation results shown in Fig. 4(b) can be regarded as the part of the rotating reference frames.

The simulation results of both models are compared with the experiments, as shown in Fig. 5(c) and (d). Even though there are small differences between simulations and experiments, the HSS modeling show the same capability with the nonlinear time-domain simulations. The linear components are only implemented in the simulations. Furthermore, the dead time and the nonlinear characteristic of the passive elements are not considered in the HSS model. Hence, the even-order harmonics, which are normally driven by the dead time, and the coupling effect of them to other harmonics are not shown in the HSS model and PLECS as well.

Also, the frequency at the ac side is shown at the dc side as a shifted frequency or a coupled frequency according to the components in switching, ac, and dc sides, and it is transferred again to the ac side. For instance, even-order harmonics at the ac side will be shown at the dc side as odd-order harmonics, and it will be shown again as even-order harmonics of the ac side. However, both odd- and even-order harmonics move simultaneously in practical systems, and it makes different magnitudes of harmonics. Hence, this coupled behavior makes an error if one component is not considered in the analytical model as well as in the nonlinear time-domain simulation.

C. *Short Discussion About the Effect of the FC and the SIV*

Power converters used in the grid have generally four parts: the dc network, the ac network, the controller, and the switching network. The ac current (i_{ac}) from the ac network is modulated by switches (insulated-gate bipolar transistors or MOSFETs) to result in dc current (i_{dc}). The dc network then transforms the dc current to the dc voltage (v_{dc}), and it is converted to

the ac-side voltage ($v_{\rm ac}$). The derived ac voltage result in an ac current change by interacting with the ac system source and impedance. This iterative procedure creates a feedback loop, which governs the overall system response. However, if the procedure is assumed that the dc-side voltage is independent of the dc-side current, the model can be simplified for linearization and analysis like SSAV. Furthermore, GAV can be considered in the modeling by assuming that positive and negative sequences are dominant in the analysis. Additionally, positive sequence can only be considered for the analysis of systems by separating the positive sequence into real part (*D*-axis) and imaginary part (*Q*-axis). However, this simplification is not easily acceptable for the analysis of harmonic interaction due to the FC. For instance, if the frequency component of the ac grid current contains f_g and the modulation frequency includes f_m, the coupled frequencies $f_g + f_m$ and $f_g - f_m$ will be appeared on the dc-side current. It will then be transferred back to the the ac side after convoluting with the dc side. As a result, the consideration of the FC make the model include the dc-side impedance at a different frequency by closing a feedback loop. These coupled frequencies may be transferred to another connected converter and be involved in another FC. Conclusively, the HSS model tries to include all FC behavior by adjusting the number of harmonics, while the conventional methods (SSAV, DQ, and GAV) do not or partially consider the impedance driven by the FC due to their basic assumption used in the modeling procedure. The importance of considering the FC may be more critical as the number of converters considered in the modeling increases.

Any distortion to power converters may cause SIVs, where transient behaviors and nonharmonic frequencies can be regarded as the distortions. They are transferred into the switching behavior through the SIV particularly by adding frequency components, which are related to the distortion frequencies. The control action from the measured variables generates the SIV, and any small variation of measured variable will propagate through the control response and result in the SIV in the controlled converter. These variations generate many frequencies, and, in general, the control response should be optimized by taking all these frequencies into account [54], [55]. For instance, the output vector ($Y_{fc} = [\Delta \mathrm{SW}_A \ \Delta \mathrm{SW}_B \ \Delta \mathrm{SW}_C]^T$) of (32) in the paper can be regarded as the SIV, which contains the propagated frequency information from the controller. Conclusively, both the FC and the SIV are important criteria that have to be considered in the modeling to analyze the harmonic interaction accurately. It is worth to note that full characteristics of them can only be included in the modeling by using the HSS method.

V. Conclusion

This paper analyzes the harmonic interaction between the grid-connected converter and the grid voltage by using the HSS modeling. First, the full HSS modeling procedure is provided to show the difference to the conventional modeling methods. Second, the output results from the developed model are compared with the nonlinear time-domain simulation result to show the validity of the HSS model. The results obtained with the HSS model are well matched with the ones obtained with a commercial simulation tool and with experimental results. Third, the HSS model is used as a tool to analyze the steady-state harmonic interaction as well as the dynamic harmonic interaction. The result shows how harmonics are transferred in the model and which impedances are effective to generate the harmonics.

The result from the HSS model can be used to give accurate results compared to the conventional simulation results. Furthermore, the derived harmonic coupling matrix can be extended to the FC analysis with other connected devices.

References

[1] J. Kwon, X. Wang, C. L. Bak, and F. Blaabjerg, "Harmonic interaction analysis in grid connected converter using harmonic state space (HSS) modeling," in *Proc. IEEE Appl. Power Electron. Conf. Expo.*, 2015, pp. 1779–1786.

[2] J. H. R. Enslin and P. J. M. Heskes, "Harmonic interaction between a large number of distributed power inverters and the distribution network," *IEEE Trans. Power Electron.*, vol. 19, no. 6, pp. 1586–1593, Nov. 2004.

[3] M. Bollen *et al.*, "Future work on harmonics—Some expert opinions—Part I: Wind and solar power," in *Proc. IEEE 16th Int. Conf. Harmonics Quality Power*, 2014, pp. 904–908.

[4] J. Meyer *et al.*, "Future work on harmonics—Some expert opinions—Part II: Supraharmonics, standards and measurements," in *Proc. IEEE 16th Int. Conf. Harmonics Quality Power*, 2014, pp. 909–913.

[5] X. Wang, F. Blaabjerg, and W. Wu, "Modeling and analysis of harmonic stability in an AC power-electronics-based power system," *IEEE Trans. Power Electron.*, vol. 29, no. 12, pp. 6421–6432, Dec. 2014.

[6] X. Wang, F. Blaabjerg, M. Liserre, Z. Chen, J. He, and Y. Li, "An active damper for stabilizing power-electronics-based AC systems," *IEEE Trans. Power Electron.*, vol. 29, no. 7, pp. 3318–3329, Jul. 2014.

[7] S. T. Tentzerakis and S. A. Papathanassiou, "An investigation of the harmonic emissions of wind turbines," *IEEE Trans. Energy Convers.*, vol. 22, no. 1, pp. 150–158, Mar. 2007.

[8] A. Petersson, T. Thiringer, L. Harnefors, and T. Petru, "Modeling and experimental verification of grid interaction of a DFIG wind turbine," *IEEE Trans. Energy Convers.*, vol. 20, no. 4, pp. 878–886, Dec. 2005.

[9] S. Liang, Q. Hu, and W. J. Lee, "A survey of harmonic emissions of a commercially operated wind farm," *IEEE Trans. Ind. Appl.*, vol. 48, no. 3, pp. 1115–1123, May 2012.

[10] J. Sun, "Small-signal methods for AC distributed power systems: A review," *IEEE Trans. Power Electron.*, vol. 24, no. 11, pp. 2545–2554, Nov. 2009.

[11] X. Feng, J. Liu, and F. C. Lee, "Impedance specifications for stable DC distributed power systems," *IEEE Trans. Power Electron.*, vol. 17, no. 2, pp. 157–162, Mar. 2002.

[12] S. R. Kaprielian, A. E. Emanuel, R. V. Dwyer, and H. Mehta, "Predicting voltage distortion in a system with multiple random harmonic sources," *IEEE Trans. Power Del.*, vol. 9, no. 3, pp. 1632–1638, Jul. 1994.

[13] D. G. Infield, P. Onions, A. D. Simmons, and G. A. Smith, "Power quality from multiple grid-connected single-phase inverters," *IEEE Trans. Power Del.*, vol. 19, no. 4, pp. 1983–1989, Oct. 2004.

[14] X. Wang, F. Blaabjerg, and Z. Chen, "Autonomous control of inverter-interfaced distributed generation units for harmonic current filtering and resonance damping in an islanded microgrid," *IEEE Trans. Ind. Appl.*, vol. 50, no. 1, pp. 452–461, Jan. 2014.

[15] S. R. Sanders, J. M. Noworolski, X. Z. Liu, and G. C. Verghese, "Generalized averaging method for power conversion circuits," *IEEE Trans. Power Electron.*, vol. 6, no. 2, pp. 251–259, Apr. 1991.

[16] P. Mattavelli, A. M. Stankovic, and G. C. Verghese, "SSR analysis with dynamic phasor model of thyristor-controlled series capacitor," *IEEE Trans. Power Syst.*, vol. 14, no. 1, pp. 200–208, Feb. 1999.

[17] D. J. Perreault and G. C. Verghese, "Time-varying effects and averaging issues in models for current-mode control," *IEEE Trans. Power Electron.*, vol. 12, no. 3, pp. 453–461, May 1997.

[18] J. R. C. Orillaza and A. R. Wood, "Harmonic state-space model of a controlled TCR," *IEEE Trans. Power Del.*, vol. 28, no. 1, pp. 197–205, Jan. 2013.

[19] M. S.-P. Hwang and A. R. Wood, "A new modelling framework for power supply networks with converter based loads and generators—The

harmonic state-space," in *Proc. IEEE Int. Conf. Power Syst. Technol.*, 2012, pp. 1–6.
[20] S. Vesti, T. Suntio, J. Á. Oliver, R. Prieto, and J. A. Cobos, "Effect of control method on impedance-based interactions in a buck converter," *IEEE Trans. Power Electron.*, vol. 28, no. 11, pp. 5311–5322, Nov. 2013.
[21] M. Cespedes and J. Sun, "Impedance modeling and analysis of grid-connected voltage-source converters," *IEEE Trans. Power Electron.*, vol. 29, no. 3, pp. 1254–1261, Mar. 2014.
[22] J. Sun, "Impedance-based stability criterion for grid-connected inverters," *IEEE Trans. Power Electron.*, vol. 26, no. 11, pp. 3075–3078, Nov. 2011.
[23] J. Sun, Z. Bing, and K. J. Karimi, "Input impedance modeling of multipulse rectifiers by harmonic linearization," *IEEE Trans. Power Electron.*, vol. 24, no. 12, pp. 2812–2820, Dec. 2009.
[24] J. Sun and Z. Bing, "Input impedance modeling of single-phase PFC by the method of harmonic linearization," in *Proc. 23rd Annu. IEEE Appl. Power Electron. Conf. Expo.*, 2008, pp. 1188–1194.
[25] K. Ilves, A. Antonopoulos, S. Norrga, and H. P. Nee, "Steady-state analysis of interaction between harmonic components of arm and line quantities of modular multilevel converters," *IEEE Trans. Power Electron.*, vol. 27, no. 1, pp. 57–68, Jan. 2012.
[26] X. Yuan and A. Lovett, "Dc-link capacitance reduction in a high power medium voltage modular wind power converter," in *Proc. 15th Eur. Conf. Power Electron. Appl.*, 2013, pp. 1–10.
[27] Y. Zhang and Y. W. Li, "Investigation and suppression of harmonics interaction in high-power PWM current-source motor drives," *IEEE Trans. Power Electron.*, vol. 30, no. 2, pp. 668–679, Feb. 2015.
[28] E. Acha, A. Semlyen, and N. Rajakovic, "A harmonic domain computational package for nonlinear problems and its application to electric arcs," *IEEE Trans. Power Del.*, vol. 5, no. 3, pp. 1390–1397, Jul. 1990.
[29] M. Madrigal and E. Acha, "Modelling of custom power equipment using harmonic domain techniques," in *Proc. 9th Int. Conf. Harmonics Quality Power*, 2000, vol. 1, pp. 264–269.
[30] J. Arrillaga and N. R. Watson, "The harmonic domain revisited," in *Proc. 13th Int. Conf. Harmonics Quality Power*, 2008, pp. 1–9.
[31] J. J. Rico, E. Acha, and T. J. E. Miller, "Harmonic domain modelling of three phase thyristor-controlled reactors by means of switching vectors and discrete convolutions," *IEEE Trans. Power Del.*, vol. 11, no. 3, pp. 1678–1684, Jul. 1996.
[32] J. J. Rico, M. Madrigal, and E. Acha, "Dynamic harmonic evolution using the extended harmonic domain," *IEEE Trans. Power Del.*, vol. 18, no. 2, pp. 587–594, Apr. 2003.
[33] B. Vyakaranam, M. Madrigal, F. E. Villaseca, and R. Rarick, "Dynamic harmonic evolution in FACTS via the extended harmonic domain method," in *Proc. Power Energy Conf. Illinois*, 2010, pp. 29–38.
[34] S. M. Mazhari, S. M. Kouhsari, A. Ramirez, and E. Karami, "Interfacing transient stability and extended harmonic domain for dynamic harmonic analysis of power systems," *IET Gener. Transmiss. Distrib.*, vol. 10, no. 11, pp. 2720–2730, 2016.
[35] U. Vargas and A. Ramirez, "Reformulating extended harmonic domain models for accurate representation of harmonics dynamics," *IEEE Trans. Power Del.*, vol. 31, no. 6, pp. 2562–2564, Dec. 2016.
[36] U. Vargas and A. Ramirez, "Extended harmonic domain model of a wind turbine generator for harmonic transient analysis," *IEEE Trans. Power Del.*, vol. 31, no. 3, pp. 1360–1368, Jun. 2016.
[37] F. Yahyaie and P. W. Lehn, "On dynamic evaluation of harmonics using generalized averaging techniques," *IEEE Trans. Power Syst.*, vol. 30, no. 5, pp. 2216–2224, Sep. 2015.
[38] J. de, J. Chavez, and A. Ramirez, "Assessment of harmonic resonances in switched networks," *IEEE Trans. Power Del.*, vol. 26, no. 3, pp. 2058–2059, Jul. 2011.
[39] G. N. Love and A. R. Wood, "Harmonic state space model of power electronics," in *Proc. 13th Int. Conf. Harmonics Quality Power*, 2008, pp. 1–6.
[40] M. S. Hwang and A. R. Wood, "Harmonic state-space modelling of an HVdc converter," in *Proc. IEEE 15th Int. Conf. Harmonics Quality Power*, 2012, pp. 573–580.
[41] E. Karami, G. B. Gharehpetian, and M. Madrigal, "A step forward in application of dynamic harmonic domain: Phase shifting property of harmonics," *IEEE Trans. Power Del.*, 2016, to be published.
[42] A. Ramirez, "Reduced-order state-space systems in the dynamic harmonic domain," in *Proc. 16th Int. Conf. Harmonics Quality Power*, 2014, pp. 773–777.
[43] J. J. Chavez, A. Ramirez, and V. Dinavahi, "Dynamic harmonic domain modelling of synchronous machine and transmission line interface," *IET Gener. Transmiss. Distrib.*, vol. 5, no. 9, pp. 912–920, Sep. 2011.
[44] J. R. Orillaza, M. S. P. Hwang, and A. R. Wood, "Switching instant variation in harmonic state-space modelling of power electronic devices," in *Proc. 20th Australasian Univ. Power Eng. Conf.*, 2010, pp. 1–5.
[45] E. Mollerstedt and B. Bernhardsson, "A harmonic transfer function model for a diode converter train," in *Proc. IEEE Power Eng. Soc. Winter Meeting*, 2000, vol. 2, pp. 957–962.
[46] E. Mollerstedt and B. Bernhardsson, "Out of control because of harmonics—An analysis of the harmonic response of an inverter locomotive," *IEEE Control Syst.*, vol. 20, no. 4, pp. 70–81, Aug. 2000.
[47] N. M. Wereley and S. R. Hall, "Frequency response of linear time periodic systems," in *Proc. 29th IEEE Conf. Decision Control*, 1990, vol. 6, pp. 3650–3655.
[48] N. M. Wereley and S. R. Hall, "Linear time periodic systems: Transfer function, poles, transmission zeroes and directional properties," in *Proc. Amer. Control Conf.*, 1991, pp. 1179–1184.
[49] S. R. Hall and N. M. Wereley, "Generalized Nyquist stability criterion for linear time periodic systems," in *Proc. Amer. Control Conf.*, 1990, pp. 1518–1525.
[50] J. B. Kwon, X. Wang, F. Blaabjerg, C. L. Bak, A. R. Wood, and N. R. Watson, "Harmonic instability analysis of a single-phase grid-connected converter using a harmonic state-space modeling method," *IEEE Trans. Ind. Appl.*, vol. 52, no. 5, pp. 4188–4200, Sep. 2016.
[51] R. Tymerski, "Application of the time-varying transfer function for exact small-signal analysis," *IEEE Trans. Power Electron.*, vol. 9, no. 2, pp. 196–205, Mar. 1994.
[52] R. Tymerski, "Frequency analysis of time-interval-modulated switched networks," *IEEE Trans. Power Electron.*, vol. 6, no. 2, pp. 287–295, Apr. 1991.
[53] D. G. Holmes and T. A. Lipo, *Pulse Width Modulation for Power Converters: Principles and Practice*. New York, NY, USA: Wiley-IEEE Press, 2003.
[54] B. Wen, D. Boroyevich, R. Burgos, P. Mattavelli, and Z. Shen, "Small-signal stability analysis of three-phase AC systems in the presence of constant power loads based on measured d-q frame impedances," *IEEE Trans. Power Electron.*, vol. 30, no. 10, pp. 5952–5963, Oct. 2015.
[55] S. Lissandron, L. D. Santa, P. Mattavelli, and B. Wen, "Experimental validation for impedance-based small-signal stability analysis of single-phase interconnected power systems with grid-feeding inverters," *IEEE J. Emerg. Sel. Topics Power Electron.*, vol. 4, no. 1, pp. 103–115, Mar. 2016.

JunBum Kwon (S'14) was born in Seoul, South Korea, in 1982. He received the B.S. and M.S. degrees in control and instrumentation engineering from Seoul National University of Science and Technology, Seoul, in 2007 and 2010, respectively. He is currently working toward the Ph.D. degree with the Department of Energy Technology, Aalborg University, Aalborg, Denmark.

He was an Research Engineer with the HVDC Rsearch and Development Center, LS Industrial Systems, Anayang, South Korea, from 2010 to 2013. His research interests include three-phase grid-connected inverter for renewable energy, harmonic analysis with modeling, insulation coordination design, and thyristor valve design for high-voltage dc.

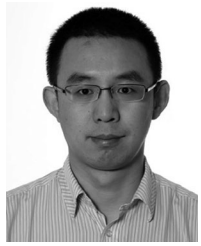

Xiongfei Wang (S'10–M'13) received the B.S. degree from Yanshan University, Qinhuangdao, China, in 2006, the M.S. degree from Harbin Institute of Technology, Harbin, China, in 2008, both in electrical engineering, and the Ph.D. degree with the Department of Energy Technology, from Aalborg University, Aalborg, Denmark, in 2013.

Since 2009, he has been with Aalborg University, where he is currently an Associate Professor with the Department of Energy Technology. His research interests include modeling and control of grid-connected converters, harmonics analysis and control, passive and active filters, and stability of power-electronic-based power systems.

Dr. Wang received the IEEE POWER ELECTRONICS TRANSACTIONS Prize Paper award in 2014. He is an Associate Editor for the IEEE TRANSACTIONS ON INDUSTRY APPLICATIONS and the IEEE JOURNAL OF EMERGING AND SELECTED TOPICS IN POWER ELECTRONICS.

Frede Blaabjerg (S'86–M'88–SM'97–F'03) received the Ph.D. degree with the Department of Energy Technology from Aalborg University, Aalborg, Denmark.

He was with ABB-Scandia, Randers, Denmark, from 1987 to 1988. He became an Assistant Professor in 1992, an Associate Professor in 1996, and a Full Professor of power electronics and drives in 1998 at Aalborg University. His current research interests include power electronics and its applications, such as wind turbines, photovoltaic systems, reliability, harmonics, and adjustable speed drives.

Dr. Blaabjerg has received 17 IEEE Prize Paper Awards, the IEEE Power Electronics Society Distinguished Service Award in 2009, the EPE-PEMC Council Award in 2010, the IEEE William E. Newell Power Electronics Award 2014, and the Villum Kann Rasmussen Research Award 2014. He was an Editor-in-Chief of the IEEE TRANSACTIONS ON POWER ELECTRONICS from 2006 to 2012. He was nominated in 2014 and 2015 by Thomson Reuters to be among the most 250 cited researchers in Engineering in the world.

Claus Leth Bak (SM'07) was born in Århus, Denmark, on April 13, 1965. He received the B.Sc. (Hons.) degree in electrical power engineering in 1992, the M.Sc. degree in electrical power engineering from the Department of Energy Technology, Aalborg University, Aalborg, Denmark, in 1994, and the Ph.D. degree in energy technology from Aalborg University in 2015 with the thesis entitled "EHV/HV underground cables in the transmission system."

He then worked as a Professional Engineer with Electric Power Transmission and Substations with specializations within the area of power system protection at the NV Net Transmission Company. In 1999, he became an Assistant Professor at the Department of Energy Technology, Aalborg University, where he is currently a Full Professor. He serves as the Head of the Energy Technology Ph.D. program (more than 100 Ph.D.'s) and as the Head of the Section of Electric Power Systems and High Voltage at Aalborg University, where he is also a member of the Ph.D. board at the Faculty of Engineering and Science. He has supervised/cosupervised more than 30 Ph.D.'s and more than 50 M.Sc. theses. He has authored/coauthored about 200 publications. His main research interests include corona phenomena on overhead lines, power system modeling and transient simulations, underground cable transmission, power system harmonics, power system protection, and high-voltage dc voltage-source converter offshore transmission networks.

Dr. Bak is a member of Cigré JWG C4-B4.38, Cigré SC C4, and SC B5 study committees and the Danish Cigré National Committee. He received the DPSP 2014 Best Paper Award and the PEDG 2016 Best Paper Award.

Vasile-Simion Sularea was born in Deva, Romania, in 1991. He received the B.S. degree in electrical engineering from the Polytechnic University of Timisoara, Timisoara, Romania, in 2014, and the M.S. degree in energy technology from Aalborg University, Aalborg, Denmark, in 2016.

He is currently a Research Assistant with the Department of Energy Technology, Aalborg University. His interests include design and control of medium-power grid-connected ac–dc converters and dc–dc converters for high-current applications.

Cristian Busca (S'10–M'13) received the M.Sc. degree in power electronics and drives, and the Ph.D. degree in reliability of power devices from Aalborg University, Aalborg, Denmark, in 2010 and 2013, respectively.

He is currently with the Department of energy technology, Aalborg University. His current research interests include design and control of high-efficiency and reliable power electronics for renewable energy.